Københavns Universitet

Solid-state QCPMG NMR of Low-γ quadrupolar metal nuclei in natural abundance

Larsen, Flemming Hofmann; Skibsted, Jørgen; J. Jakobsen, Hans; Nielsen, Niels Chr.

Solid-State QCPMG NMR of Low-γ Quadrupolar Metal Nuclei in Natural Abundance

Flemming H. Larsen,[†,§] Jørgen Skibsted,[‡] Hans J. Jakobsen,[‡] and Niels Chr. Nielsen*,[†]

Contribution from the Laboratory for Biomolecular NMR Spectroscopy, Department of Molecular and Structural Biology, Science Park, and Instrument Centre for Solid-State NMR Spectroscopy, Department of Chemistry, University of Aarhus, DK-8000 Aarhus C, Denmark

Abstract: Taking advantage of an order of magnitude in sensitivity enhancement obtained by sampling of quadrupolar-echo (QE) solid-state NMR spectra during a quadrupolar Carr−Purcell−Meiboom−Gill (QCPMG) pulse sequence, we demonstrate that the coordination environment of low-γ quadrupolar metal nuclei can be studied routinely for powders with these nuclei in natural abundance. The general applicability of the method is demonstrated by ^{39}K, ^{25}Mg, ^{67}Zn, and ^{87}Sr QCPMG solid-state NMR experiments for K_2MoO_4, KVO_3, $Mg(VO_3)_2$, $Zn(CH_3COO)_2 \cdot 2H_2O$, $Zn(Ala)_2 \cdot H_2O$, $Sr(NO_3)_2$, and $SrMoO_4$. For all samples the quadrupolar coupling parameters and the isotropic chemical shifts are extracted by numerical simulation and iterative fitting of the spin−echo sideband spectra observed in the experimental QCPMG NMR spectra. These parameters are discussed in light of the crystal structures for the compounds.

1. Introduction

Alkali and earth alkali metal ions play a fundamental role in the chemistry of many compounds ranging from semi- and superconductors, piezoelectrics, and minerals via alkalides and metalloporphyrins to metalloproteins and -enzymes responsible for vital biological functions. For example, the latter category[1,2] includes chelates such as chlorophyll A and heme being important for photosynthesis and biochemical electron-transfer reactions.[3] In the binding sites of metalloproteins, metal ions such as Zn^{2+}, Mg^{2+}, and K^+ are responsible for the catalytic/enzymatic activity or function regulation through metal-ion induced conformational changes. In fact, the catalytic activity of about 30% of all known enzymes relies on the presence of metal ions in the active sites.[4] This aspect renders metal binding an attractive target for external control/regulation of biological functions.[5] The regulation relies on the specific affinity of the metal toward various donor atoms (O, N, or S) and the local ligand symmetry.

The important role of metal ions as molecular reaction centers makes the characterization of the local structure for these ions an extremely important issue. This has prompted numerous studies of structure versus function for metal binding sites using X-ray diffraction (XRD), electron paramagnetic resonance (EPR), nuclear quadrupole resonance (NQR), liquid- as well as solid-state nuclear magnetic resonance (NMR) spectroscopy,

Mössbauer spectroscopy, and extended X-ray absorption fine structure (EXAFS) spectroscopy. For example, these methods have been used to study macromolecules of specific interests[3,6−9] as well as model systems which mimic their binding sites.[10−12] Depending on the molecular system and the particular ion subject to investigation, the different methods have clear advantages/disadvantages. For example, XRD applies to crystal-line samples, EPR to paramagnetic species, NQR to quadrupolar nuclei in solids generally exhibiting large quadrupole couplings, and liquid-state NMR to molecules with a high degree of isotropic motion, while solid-state NMR applies to molecules immobilized by size, aggregation, or coordination in crystalline or amorphous solids. Furthermore, the spectroscopic techniques differ from XRD in the sense that they may provide specific information about the local structure of the binding site for the metal ion. In addition, they allow characterization of crystalline as well as noncrystalline solids. The latter aspect opens up the possibility for studying metalloproteins in membranes.

While liquid-state NMR of metal nuclei has gained popularity in studies of metalloproteins as recently reviewed by Drakenberg et al.,[4] the use of solid-state NMR to study metal binding employing low-γ quadrupolar nuclei such as ^{25}Mg, ^{39}K, ^{67}Zn, and ^{87}Sr has been quite rare. This is ascribed to several facts. First, these nuclei have a low gyromagnetic ratio (γ) which causes low sensitivity (proportional to $\gamma^{5/2}B_0^{3/2}$) and severe probe ringing artifacts. Second, the relevant spin isotopes generally have low natural abundance which translates directly into low sensitivity unless isotope enrichment is employed. Third, the half-integer spin quadrupolar nuclei of interest have quite large quadrupole moments (Q) which may impede liquid-state NMR

---

* Address correspondence to this author.

† Laboratory for Biomolecular NMR Spectroscopy, Department of Molecular and Structural Biology.

§ Present address: Department of Earth Sciences, University of Cambridge, CB2 3EQ Cambridge, United Kingdom.

‡ Instrument Centre for Solid-State NMR Spectroscopy, Department of Chemistry.

(1) Fraisto da Silva, J. J. R.; Williams, R. J. P. *The Biological Chemistry of the Elements*; Clarendon Press: Oxford, 1991.

(2) Christianson, D. W. *Adv. Protein Chem.* **1991**, *42*, 281.

(3) Utschig, L. M.; Ohigashi, Y.; Thurnauer, M. C.; Tiede, D. M. *Biochemistry* **1998**, *37*, 8278.

(4) Drakenberg, T.; Johansson, C.; Forsen, S. Metal NMR for the Study of Metalloproteins. In *Methods in Molecular Biology, Vol. 60: Protein NMR Techniques*; Reid, D. G., Ed.; Humana Press: Totowa, NJ, 1997.

(5) Suzuki, K.; Hiroaki, H.; Kohda, D.; Nakumura, H.; Tanaka, T. *J. Am. Chem. Soc.* **1998**, *120*, 13008.

(6) Christianson, D. W.; Libscomb, W. N. *Acc. Chem. Res.* **1989**, *22*, 62.

(7) Kennedy, M. A.; Ellis, P. D. *J. Am. Chem. Soc.* **1989**, *111*, 3195.

(8) Bentrop, D.; Bertini, I.; Cremonini, M. A.; Forsen, S.; Luchinat, C.; Malmendal, A. *Biochemistry* **1997**, *36*, 11605.

(9) Scrofani, S. D.; Wright, P. E.; Dyson, H. J. *Protein Sci.* **1998**, *7*, 2476.

(10) Ellis, P. D. *Science* **1983**, *221*, 1141.

(11) Larsen, F. H.; Lipton, A. S.; Jakobsen, H. J.; Nielsen, N. C.; Ellis, P. D. *J. Am. Chem. Soc.* **1999**, *121*, 3783.

(12) Hammes, B. S.; Carrano, C. J. *Inorg. Chem.* **1999**, *38*, 4593.

Table 1. NMR Properties for ^{39}K, ^{25}Mg, ^{67}Zn, and ^{87}Sr[13]

isotope	spin quantum no.	natural abund. (%)	gyromagnetic ratio γ (10^7 rad T^{-1} s^{-1})	Larmor freq[a] $\omega_0/2\pi$ (MHz)	quadrupole moment Q (10^{28} m^{-2})
^{39}K	3/2	93.26	1.2498	27.996	0.049
^{25}Mg	5/2	10.00	−1.639	36.711	0.201
^{67}Zn	5/2	4.11	1.6738	37.525	0.150
^{87}Sr	9/2	7.00	−1.163	26.001	0.335

a Larmor frequencies at a static magnetic field strength of 14.1 T.

studies of these nuclei and may give rise to very broad solid-state NMR second-order powder patterns. Fourth, low-γ quadrupolar nuclei may occasionally be associated with quite long T_1 relaxation times rendering signal averaging very time-consuming. These aspects, summarized for ^{39}K, ^{25}Mg, ^{67}Zn, and ^{87}Sr in Table 1,[13] make solid-state NMR studies of these nuclei technically demanding and associated with very low sensitivity. The above difficulties have motivated studies where the metal ion has been exchanged with a spin $I = \frac{1}{2}$ metal nucleus giving a more favorable NMR response such as ^{113}Cd.[10,14,15] As has been generally stated, this approach only serves as a model for the metalloprotein structure since the cation exchange may cause changes of the local structure under investigation.

For solid-state NMR to be a general tool for low-γ quadrupolar nuclei in studies of metal binding sites, it is necessary that the problems concerning sensitivity and probe ringing be effectively solved to (i) study the active sites in biomolecular systems potentially using isotope labeling and (ii) routinely examine the impact of the type/number of donor atoms and ligand symmetry on the chemical shielding and quadrupolar coupling interaction parameters using nonlabeled model compounds. The latter aspect is of fundamental importance since, with the lack of reliable quadrupolar coupling parameters in solids from ab initio or density functional theory calculations, the only reliable route to extract detailed structural information from solid-state NMR experiments by necessity is based on empirical or semiempirical correlations between NMR parameters and known model structures.

So far the most widely appreciated step toward NMR on low-γ quadrupolar nuclei has been undertaken by the development of high-field solid-state NMR equipment which in combination with sampling using a quadrupolar-echo (QE)[16−18] reduces probe ringing effects to an extent that allows detection of ^{39}K, ^{25}Mg, and ^{67}Zn in natural abundance.[19−23] In particular this holds for compounds with these cations in relatively symmetric environments. In more general cases where the second-order quadrupolar line shape for the ($-\frac{1}{2}$, $\frac{1}{2}$) transition may extend over hundreds of kilohertz, the sensitivity is still too low for general applications. In this paper we demonstrate that this condition may be improved significantly by detecting the QE free-induction decay (FID) through a quadrupolar Carr−
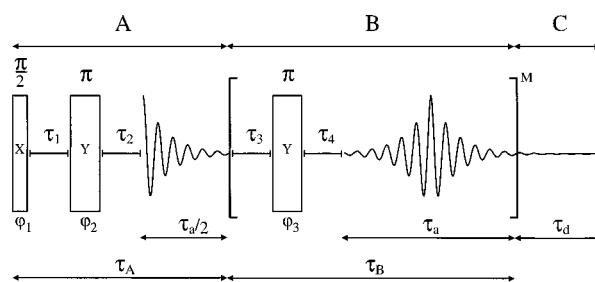

Figure 1. Timing scheme of the QCPMG pulse sequence. Part A is a quadrupolar echo (QE) element with τ_2 adjusted such that the acquisition starts at the echo maximum. Part B is the *M*-time repeating unit containing the central-transition selective π refocusing pulse followed by sampling of the echo in a period τ_a. The bracketing delays τ_3 and τ_4 protect the receiver from pulse breakthrough (note $\tau_2 - \tau_1 = \tau_4 - \tau_3$). In part C the last ($M + 1$) echo sampling period is extended by a period τ_d to ensure detection of the full decay of the FID. The pulses are phase cycled as described in ref 26.

Purcell−Meiboom−Gill (QCPMG) train of refocusing pulses.[24,25] In this manner the sensitivity may be improved by an order of magnitude[26] and baseline artifacts from probe ringing essentially removed. This opens up for routine applications as demonstrated in this work by experiments and numerical analysis of ^{25}Mg, ^{39}K, ^{67}Zn, and ^{87}Sr QCPMG spectra for powders of various inorganic, organic, and bioinorganic solids with naturally abundant spin isotopes.

2. Experimental Section

NMR Measurements. The ^{39}K, ^{25}Mg, ^{67}Zn, and ^{87}Sr NMR spectra were recorded at ambient temperature using a wide-bore Varian Unity-INOVA 600 (14.1 T) spectrometer equipped with a wideband 5 mm Varian static-powder probe. The QCPMG pulse sequence (Figure 1) was used with 1 s relaxation delay (16 s for K_2MoO_4), central-transition selective π/2 and π pulses (pulse lengths scaled by $(I + \frac{1}{2})^{-1}$ in the regime of $2\pi C_Q/(4I(2I - 1)\omega_{rf}) > 3$) of amplitude $\omega_{rf}/2\pi = 45-60$ kHz, and τ_1, τ_2, τ_3, and τ_4 spin−echo delays in the order of $40-140$ μs to minimize effects from probe ringing. The interpulse acquisition period τ_a was adjusted to obtain an appropriate sideband separation ($1/\tau_a$) ensuring a significant sensitivity enhancement while maintaining the details of the envelope for the second-order quadrupolar powder pattern. This is required for a precise determination of the quadrupolar coupling constant (C_Q) and the asymmetry parameter (η_Q) from numerical simulation and iterative fitting to the experimental spin−echo sideband patterns. The ^{39}K, ^{25}Mg, ^{67}Zn, and ^{87}Sr NMR spectra are referenced to external aqueous solutions of 1.0 M KCl, 3.0 M $MgSO_4$, 2.0 M Zn-$(NO_3)_2$, and 1.0 M $SrCl_2$, respectively. Spectral simulations and iterative fitting were performed on a 450 MHz Pentium III processor using the procedures described elsewhere.[26,27] Specifically, the iterative fitting evaluates the root-mean-square deviation between integrated spin−echo sideband intensities from experimental and calculated QCPMG spectra. The QCPMG spectra were calculated taking into consideration effects from finite radio frequency pulses: (i) in the initial stages of the iterative fitting the full QCPMG FID was approximated by a FID generated through replication of the FID from the $M = 1$ part of the pulse sequence in Figure 1 (calculated using finite rf pulses) M times and (ii) in the final stages of the iterative fitting the full QCPMG FID was approximated by taking the finite pulse effects from all radio frequency pulses fully into account.[26,27]

Materials. Powder samples of K_2MoO_4, KVO_3, Zn(CH_3COO)$_2$·$2H_2O$, and Sr(NO_3)$_2$ were obtained commercially and used without further purification. Zn(CH_3CHNH_2COO)$_2$·xH_2O (Zn(Ala)$_2$·xH_2O) was synthesized by dissolving L-alanine and ZnO (molar ratio 1.9:1) in

(13) *Table of Isotopes*; Firestone, R. B., Shirley, V. S., Eds.; John Wiley and Sons: New York, 1996.

(14) Honkonen, R. S.; Ellis, P. D. *J. Am. Chem. Soc.* **1984**, *106*, 5488.

(15) Lipton, A. S.; Mason, S. S.; Myers, S. M.; Reger, D. L.; Ellis, P. D. *Inorg. Chem.* **1996**, *35*, 7111.

(16) Hahn, E. L. *Phys. Rev.* **1950**, *80*, 580.

(17) Solomon, I. *Phys. Rev.* **1958**, *110*, 61.

(18) Davis, J. H.; Jeffrey, K. R.; Bloom, M.; Valic, M. I.; Higgs, T. P. *Chem. Phys. Lett.* **1976**, *42*, 390.

(19) Kunwar, A. C.; Turner, G. L.; Oldfield, E. *J. Magn. Reson.* **1986**, *69*, 124.

(20) Bastow, T. J.; Stuart, S. N. *Z. Naturforsch.* **1990**, *45A*, 459 and references sited herein.

(21) Kim, J.; Eglin, J. L.; Ellaboudy, A. S.; McMills, L. E. H.; Huang, S.; Dye, J. L. *J. Phys. Chem.* **1996**, *100*, 2885.

(22) Dupree, R.; Smith, M. E. *J. Chem. Soc., Chem. Commun.* **1988**, 1483.

(23) Wu, G. *Chem. Phys. Lett.* **1998**, *298*, 375.

(24) Carr, H. Y.; Purcell, E. M. *Phys. Rev.* **1954**, *94*, 630.

(25) Meiboom, S.; Gill, D. *Rev. Sci. Instrum.* **1958**, *29*, 688.

(26) Larsen, F. H.; Jakobsen, H. J.; Ellis, P. D.; Nielsen, N. C. *J. Phys. Chem. A* **1997**, *101*, 8597.

(27) Larsen, F. H.; Jakobsen, H. J.; Ellis, P. D.; Nielsen, N. C. *Mol. Phys.* **1998**, *95*, 1185.
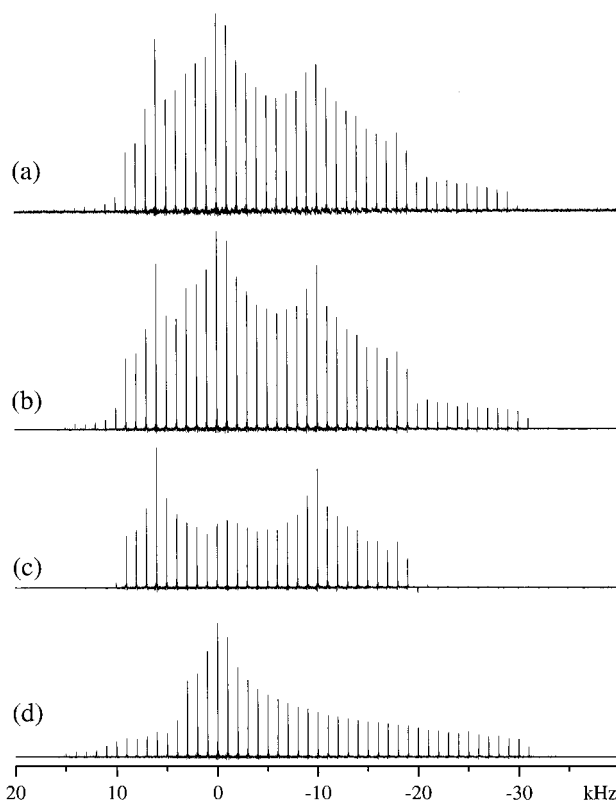
Figure 2. Experimental (a) and simulated (b−d) ^{39}K QCPMG spectra of K$_2$MoO$_4$. The experimental spectrum was recorded using $\tau_1 = \tau_3 = 40.0\ \mu s$, $\tau_2 = \tau_4 = 42.5\ \mu s$, $\tau_a = 1.0$ ms, $\tau_d = 1.188$ ms, $\omega_{rf}/2\pi = 48.8$ kHz, $M = 60$, a dwell time of 4.0 μs, and 529 scans. The simulated spectrum (b) represents the sum of the separate simulations for sites 1 (c) and 2 (d) which correspond to the parameters in Table 2. The spectra were apodized by Lorentzian line broadenings of (a) 7 and (b−d) 10 Hz.

boiling water followed by slow evaporation of the water at room temperature until crystallization begins. Finally, the complex was isolated by slow evaporation at 4 °C.[28] The purity and stoichiometry x = 1 of the sample were determined by ^{13}C and ^{1}H solid-state NMR, respectively. SrMoO$_4$ was synthesized by heating equimolar amounts of SrCO$_3$ and MoO$_3$ at 700 °C for 24 h while Mg(VO$_3$)$_2$ was prepared as described recently.[32] The basic structure and purity of SrMoO$_4$ and Mg(VO$_3$)$_2$ were confirmed by powder XRD and by ^{95}Mo and ^{51}V magic-angle-spinning (MAS) NMR.

Results and Discussion

Of the low-γ quadrupolar metal cations studied in this work, ^{39}K possesses the most favorable NMR properties (i.e., 93.26% natural abundance and a relatively low quadrupole moment). Nevertheless, ^{39}K still remains quite challenging for solid-state NMR investigations. Figure 2a shows an experimental ^{39}K QCPMG solid-state NMR spectrum of K$_2$MoO$_4$, which through the characteristic second-order quadrupolar spin−echo sideband manifolds reflects the electric field gradients and thereby the electronic surroundings of the K$^+$ ions in this compound. It is evident, as described earlier in the context of static powder,[11,26] MAS,[27,33] and multiple-quantum (MQ) MAS[34,35] NMR of half-integer quadrupolar nuclei and measurement of molecular

Table 2. Quadrupole Coupling (C_Q, η_Q) and Isotropic Chemical Shift (δ_{iso}) Parameters Determined by Iterative Fitting of ^{39}K, ^{25}Mg, ^{67}Zn, and ^{87}Sr QCPMG Powder Spectra for a Series of Solids with These Spin Isotopes in Natural Abundance[a]

compound	site	C_Q (MHz)	η_Q	δ_{iso} (ppm)
K$_2$MoO$_4$	1	2.19 ± 0.10	0.32 ± 0.05	−9 ± 5
	2	2.32 ± 0.10	0.97 ± 0.05	10 ± 5
KVO$_3$		2.44 ± 0.10	0.80 ± 0.05	−31 ± 5
Mg(VO$_3$)$_2$		8.88 ± 0.20	0.76 ± 0.05	−0.4 ± 5
Zn(CH$_3$COO)$_2$·2H$_2$O		5.35 ± 0.10	0.86 ± 0.05	2 ± 5
Zn(Ala)$_2$·H$_2$O	1	11.9 ± 0.50	0.70 ± 0.1	110 ± 20
	2	19.0 ± 0.50	0.03 ± 0.1	273 ± 20
Sr(NO$_3$)$_2$		15.4 ± 0.2	0.03 ± 0.05	−84 ± 5
SrMoO$_4$		22.7 ± 0.2	0.03 ± 0.05	−5 ± 5

[a] Accuracies are estimated by numerical calculations and visual inspection. The ^{39}K, ^{25}Mg, ^{67}Zn, and ^{87}Sr chemical shifts (corrected for second-order quadrupolar induced shifts) are on the δ scale and referenced to 1.0 M KCl, 3.0 M MgSO$_4$, 2.0 M Zn(NO$_3$)$_2$, and 1.0 M SrCl$_2$ aqueous solutions, respectively.

dynamics for ^{2}H ($I = 1$),[36] that sampling of the FID during a QCPMG pulse sequence[24,25] (Figure 1) causes a splitting of the normal QE powder pattern into a manifold of spin−echo sidebands. This leads to a significant sensitivity enhancement compared to normal QE spectroscopy (vide infra), in full analogy to the well-established sensitivity enhancement obtained in MAS experiments which split powder patterns from, e.g., first-order quadrupolar coupling into spinning sidebands.[37]

The simulated ^{39}K QCPMG NMR spectrum for K$_2$MoO$_4$ (Figure 2b) resulting from the numerical optimization is composed of two spin−echo sideband patterns (Figure 2c,d) with equal total intensities. These patterns correspond to two types of K$^+$ sites with different electronic surroundings, as reflected by the ^{39}K quadrupolar coupling (C_Q, η_Q) and isotropic chemical shift (δ_{iso}) parameters summarized in Table 2. It should be mentioned that although the spin−echo sideband manifolds are centered around the radio frequency carrier frequency, and not around δ_{iso} as in the case for spinning sideband MAS spectra from first-order quadrupolar interactions, the optimization unambiguously resolves two resonances since an acceptable fit to the experimental spectrum requires two rather than one resonance. The identification of two distinct sites is in agreement with the crystal structure for K$_2$MoO$_4$ (monoclinic, space group $C2/m$),[38] which includes two different K$^+$ ions in the asymmetric unit, both coordinated to eight oxygen atoms. The observation of almost identical δ_{iso} and C_Q values for the two sites supports the fact that the coordination polyhedra for the two K$^+$ ions are very similar. We note that the ^{39}K quadrupolar couplings for the two sites are of similar magnitude as those obtained earlier (i.e., 0.9 MHz < C_Q < 2.7 MHz) for potassium salts, using ^{39}K single-crystal NMR[20] and NQR,[39] and for K$^+$ ions complexed by crown ethers using ^{39}K QE NMR.[19,21] A somewhat larger ^{39}K quadrupolar coupling (C_Q = 3.2 MHz) has been reported for the K$^+$monensin$^-$ complex.[19]

At this stage, it appears relevant to address in more detail the fundamental aspects of the sensitivity enhancement obtained using the QCPMG method relative to the standard QE experiment. The experimental ^{39}K QCPMG spectrum of K$_2$MoO$_4$

(28) Andersen, U. Masters Thesis, University of Aarhus, 1999.
(29) Low, B. W.; Hirchfeld, F. L.; Richards, F. M. *J. Am. Chem. Soc.* **1959**, *81*, 4412.
(30) Barrie, P. J.; Gyani, A.; Motevalli, M.; O'Brien, P. *Inorg. Chem.* **1993**, *32*, 3862.
(31) Demaret, A.; Abraham, F. *Acta Crystallogr.* **1987**, *C43*, 2067.
(32) Nielsen, U. G.; Jakobsen, H. J.; Skibsted, J. *Inorg. Chem.* **2000**, *39*, 2135.
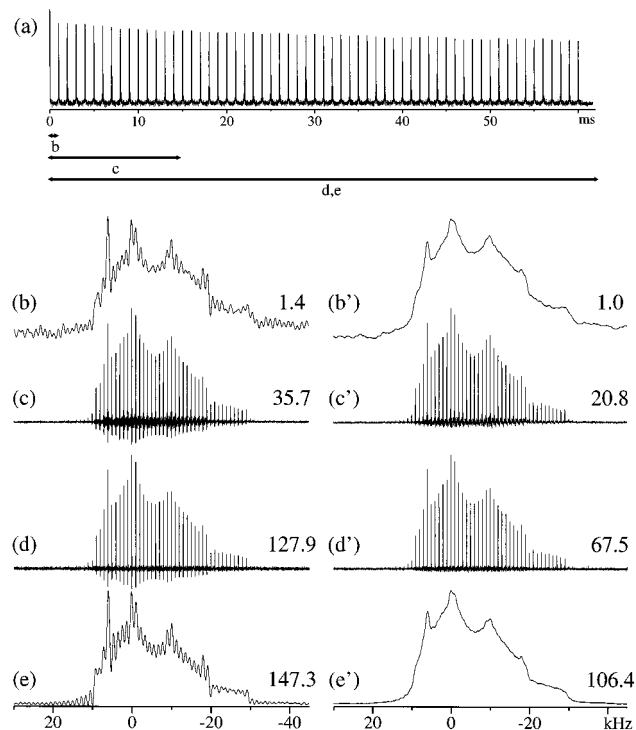(33) Larsen, F. H.; Jakobsen, H. J.; Ellis, P. D.; Nielsen, N. C. *J. Magn. Reson.* **1998**, *131*, 144.
(34) Vosegaard, T.; Larsen, F. H.; Lipton, A. S.; Jakobsen, H. J.; Nielsen, N. C.; Ellis, P. D. *J. Am. Chem. Soc.* **1997**, *119*, 9055.
(35) Larsen, F. H.; Nielsen, N. C. *J. Phys. Chem. A* **1999**, *103*, 10825.
(36) Larsen, F. H.; Jakobsen, H. J.; Ellis, P. D.; Nielsen, N. C. *Chem. Phys. Lett.* **1998**, *292*, 467.
(37) Skibsted, J.; Nielsen, N. C.; Bildsøe, H.; Jakobsen, H. J. *J. Magn. Reson.* **1991**, *95*, 88.
(38) Gatehouse, B. M.; Leverett, P. *J. Chem. Soc. A* **1969**, 849.
(39) Poplett, I. J. F.; Smith, J. A. S. *J. Chem. Soc., Faraday Trans. 2* **1981**, *77*, 1155.

QCPMG NMR of Low-γ Quadrupolar Nuclei

J. Am. Chem. Soc., Vol. 122, No. 29, 2000 7083

Figure 3. Illustration of the sensitivity enhancement obtained by QCPMG relative to QE demonstrated by different processing of the experimental spectrum from Figure 2a. (a) The full FID where the arrows indicate the part used for the transformed spectra in spectra b–e. The frequency-domain spectra were obtained by Fourier tranformation of (b, b′) the first 225 points of the FID corresponding to the decaying part of the first echo, (c, c′) the 3875 points corresponding to the first 15 echoes, (d, d′) all 15424 points corresponding to 60 echoes, and (e, e′) all 15424 points upon superposition of all half-echoes (half of them inverted with respect to time). The spectra in parts b–e were tranformed without apodization while those in parts b′–e′ used Lorentzian line broadenings of (b′, e′) 1000, (c′) 25, and (d′) 8 Hz to reduce truncation effects. The number given in the rigth-hand side of each spectrum represents the relative intensity of the spectrum.

serves as an illustrative example in this respect as demonstrated in Figure 3. The FID in Figure 3a shows that the central-transition-selective π pulses of the QCPMG experiment are indeed capable of refocusing the quadrupolar dephasing of the QE experiment. Even after a train of $M = 60$ echo pulses the magnetization has not decayed more than about 35% which immediately promises a significant sensitivity enhancement compared to sampling of the QE echo alone. This applies in particular to cases where the pulse sequence repetition rate (dictated by T_1) is much longer than the echo spacing. In the present case a relaxation delay of 16 s was used (although clearly not sufficient for full recovery of the polarization) along with an echo separation of about 1 ms. Thus, the QCPMG experiment allows sampling of $2M + 1 = 121$ half echoes in 60 ms. Neglecting the small decay of the echo amplitude, this would in terms of sensitivity correspond to 121 QE experiments each using a relaxation delay of 16 s and resulting in an equivalent experiment time of about $^1/_2$ h. Taking into account a similar repetition time for a single QCPMG experiment, the experiment time is reduced by a factor of 121 using QCPMG relative to QE. Considering the small effect from T_2 relaxation this factor could even be improved significantly by sampling more echoes in the QCPMG experiment.

These aspects become clearly apparent by comparison of the Fourier transformed spectra resulting from the QE part alone (Figure 3b,b′), the first 15 echoes of the QCPMG experiment

(Figure 3c,c′), all 60 echoes of the QCPMG experiment (Figure 3d,d′), and a spectrum generated by superposing all half echoes from the full QCPMG experiment onto the QE echo (Figure 3e,e′). In the left column of Figure 3 the spectra are Fourier transformed without apodization while the spectra in the right column are appropriately apodized to reduce sinc wiggles upon zero filling. The intensity factors written to the right of each spectrum show that the signal in the superposed spectrum in Figure 3e is 106 times more intense than that in Figure 3b, which results from the QE part of the sequence alone. This corresponds to an enhancement of the sensitivity (i.e., the signal-to-noise ratio) by a factor of 9.5 taking into account an increase in the noise by a factor of $\sqrt{121}$. Considering relaxation these numbers agree very well with the prediction given above. The QCPMG spectra using 15 and 60 echoes are 26 and 91 times more intense than the QE experiment, respectively, in the case without apodization. The apodization required to avoid sinc wiggles from the very narrow spin−echo sidebands in the QCPMG spectra (in Figure 3c the line width at half-height is 14 Hz, comparing well with the width of approximately 10 Hz for the sinc function alone) reduces the enhancement factors to 21 and 68. Although these numbers suggest that superposition of the echoes before Fourier transformation is beneficial for sensitivity reasons, several other facts are in favor of the spin−echo sideband spectra. First, by splitting the broad second-order powder spectrum into sidebands it is possible unambiguously to resolve signal components with low sensitivity from the baseline of the spectra.[27] Second, it is possible to recognize effects from homogeneous evolution due to homonuclear dipole−dipole couplings or molecular dynamics which both lead to an increased line width for the spin−echo sidebands.[36] Third, although the QCPMG experiment practically eliminates the undesirable baseline-roll effects from probe ringing, it is desirable to verify this by observing the baseline between the spin−echo sidebands which additionally provides the possibility of applying numerical baseline correction procedures.

The ^{39}K QCPMG spectrum of KVO$_3$, shown in Figure 4a, displays a QCPMG sideband manifold with an envelope that resembles a typical QE spectrum for a single ^{39}K site characterized by an asymmetry parameter about $\eta_Q \approx 0.7$ for the quadrupolar coupling interaction. From the overall width of 50 kHz for the QCPMG sideband spectrum the associated quadrupolar coupling constant may be estimated to $C_Q \approx 2.5$ MHz. Using these estimated values as initial parameters in a least-squares fit of simulated to experimental spin−echo sideband intensities gives the optimized parameters in Table 2 and the simulated spectrum in Figure 4b. The observation of a single ^{39}K resonance is in full accord with the reported orthorhombic crystal structure (space group *Pbcm*) for KVO$_3$ which contains a single K$^+$ ion in the asymmetric unit.[40] Furthermore, KVO$_3$ is isostructural with RbVO$_3$ for which ^{87}Rb quadrupole coupling and chemical shielding anisotropy (CSA) parameters for a single Rb$^+$ site recently have been determined using ^{87}Rb QCPMG NMR[26] as well as ^{87}Rb QE and single-crystal NMR.[41] The η_Q-(^{39}K) parameter for KVO$_3$ is almost identical with the value $\eta_Q(^{87}$Rb$) = 0.75 \pm 0.02$, determined for RbVO$_3$, which reflects the similar environments of the K$^+$/Rb$^+$ cations in the orthorhombic structure of these vanadates. Although a small ^{87}Rb CSA was observed for RbVO$_3$, the optimizations to the ^{39}K QCPMG spectrum showed no significant influence from a possible anisotropy for the ^{39}K shielding interaction.

The applications of ^{25}Mg solid-state NMR have so far been quite sparse and essentially limited to single-crystal studies of

(40) Hawthorne, F. C.; Calvo, C. *J. Solid State Chem.* **1977**, *22*, 157.
(41) Vosegaard, T.; Skibsted, J.; Bildsøe, H.; Jakobsen H. J. *Solid State Nucl. Magn. Reson.* **1999**, *14*, 203.
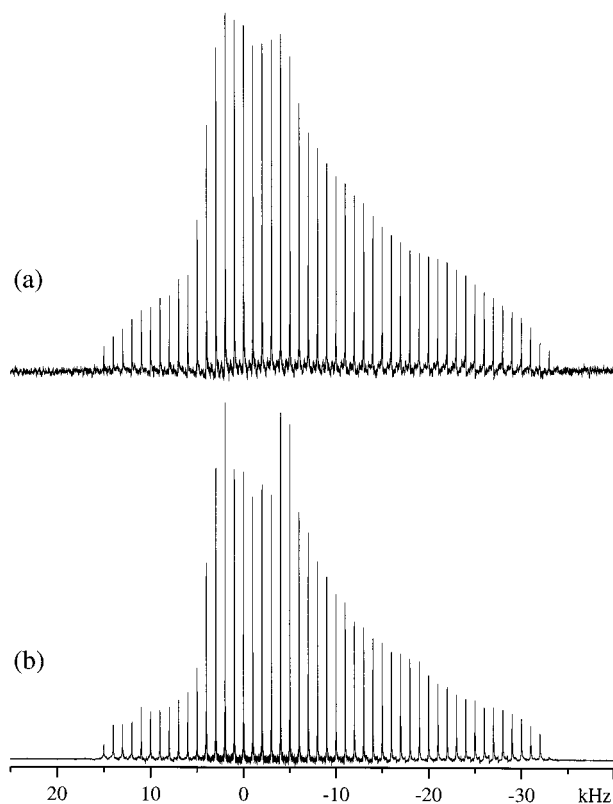
Figure 4. Experimental (a) and simulated (b) ^{39}K QCPMG spectra of KVO$_3$. The experimental spectrum was obtained using $\tau_1 = \tau_3 = 40.0$ μs, $\tau_2 = \tau_4 = 42.5$ μs, $\tau_a = 1.0$ ms, $\tau_d = 600$ μs, $\omega_{rf}/2\pi = 48.8$ kHz, $M = 30$, a dwell time of 2.0 μs, and 16384 scans. The simulated spectrum corresponds to the parameters given in Table 2. Both spectra were apodized using a 20 Hz Lorentzian line broadening.

MgF$_2$,[42] brucite (Mg(OH)$_2$),[43] and fosterite (Mg$_2$SiO$_4$)[44] and MAS or QE studies of some simple magnesium salts,[22] minerals,[45] Mg-substituted sialons,[46] and silicate melts.[47] This limited attention, seen in contrast to the importance of Mg in minerals and in biological metal binding sites, may be ascribed to the low natural abundance and low gyromagnetic ratio for ^{25}Mg and to the fact that ^{25}Mg quadrupolar couplings may be so large that MAS NMR methods hardly can be used. As an example of the applicability of QCPMG NMR in this situation, Figure 5 shows an experimental ^{25}Mg QCPMG spectrum of Mg-(VO$_3$)$_2$. The presence of spin−echo sidebands extending over some 120 kHz in this spectrum immediately demonstrates the presence of a quite large ^{25}Mg quadrupole coupling. The intensities of the experimental spin−echo sidebands may be convincingly reproduced by the numerical simulation in Figure 5b which reflects a single Mg site, characterized by the optimized C_Q, η_Q, and δ_{iso} parameters listed Table 2. This observation is in good agreement with the crystal structure for Mg(VO$_3$)$_2$ which includes a single Mg^{2+} ion, octahedrally coordinated to oxygen atoms, in the asymmetric unit.[48] So far the largest ^{25}Mg quadrupole couplings have been reported for
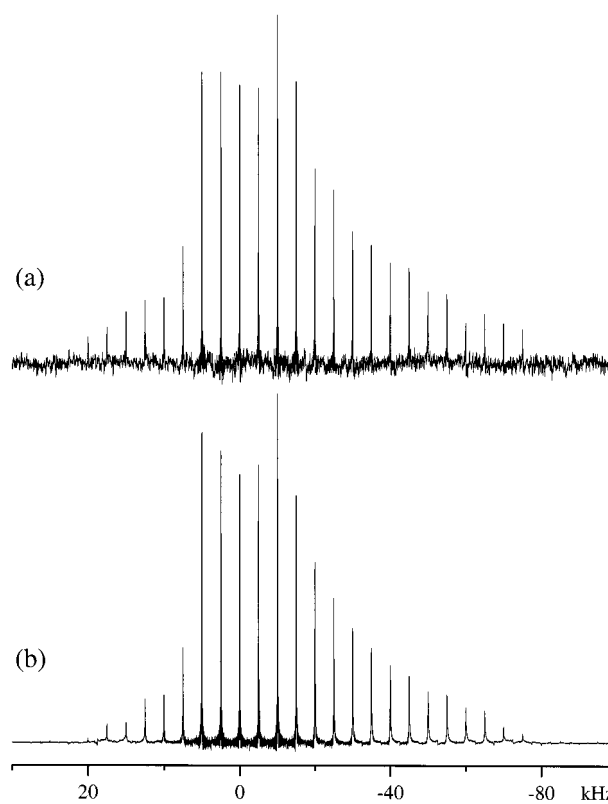
(42) Bleich, H. E.; Redfield, A. G. *J. Chem. Phys.* **1977**, *67*, 5040.
(43) Bastow, T. J. *Solid State Commun.* **1991**, *77*, 547.
(44) Derighetti, B.; Hafner, S.; Marxer, H.; Rager, H. *Phys. Lett.* **1978**, *66A*, 150.
(45) MacKenzie, K. J. D.; Meinhold, R. H. *J. Mater. Sci. Lett.* **1993**, *12*, 1696. MacKenzie, K. J. D.; Meinhold, R. H. *Thermochim. Acta* **1993**, *230*, 331. MacKenzie, K. J. D.; Meinhold, R. H. *Am. Mineral.* **1994**, *79*, 43. MacKenzie, K. J. D.; Meinhold, R. H. *Am. Mineral.* **1994**, *79*, 250. MacKenzie, K. J. D.; Meinhold, R. H. *Am. Mineral.* **1997**, *82*, 479.
(46) MacKenzei, K. J. D.; Meinhold, R. H. *J. Mater. Chem.* **1996**, *6*, 821.
(47) Fiske, P. S.; Stebbins, J. F. *Am. Mineral.* **1994**, *79*, 848.

Figure 5. Experimental (a) and simulated (b) ^{25}Mg QCPMG spectra of Mg(VO$_3$)$_2$. The experimental spectrum was obtained using $\tau_1 = 50.0$ μs, $\tau_2 = 51.6$ μs, $\tau_3 = 40.0$ μs, $\tau_4 = 41.6$ μs, $\tau_a = 200$ μs, $\tau_d = 157$ μs, $\omega_{rf}/2\pi = 52.9$ kHz, $M = 30$, a dwell time of 0.5 μs, and 65536 scans. The simulated spectrum corresponds to the parameters given in Table 2. The spectra were apodized using Lorentzian line broadenings of (a) 50 and (b) 75 Hz.

the two Mg sites in fosterite ($C_Q = 4.313$ and 4.996 MHz) from ^{25}Mg single-crystal NMR.[44] The quadrupole coupling constant of 8.88 MHz, observed for Mg(VO$_3$)$_2$ in this study, is significantly larger than these values, thereby illustrating the potential of the QCPMG experiment for extracting large quadrupolar couplings from powdered samples.

The gyromagnetic ratios and quadrupole moments for ^{25}Mg and ^{67}Zn are quite similar, the main difference being the lower natural abundance for ^{67}Zn. Again these unfavorable NMR properties may explain the limited number of ^{67}Zn solid-state NMR studies reported in the literature. These have included ^{67}Zn single-crystal,[49,50] QE,[23,51] and MAS[52,53] NMR studies of some simple inorganic solids (i.e., ZnO,[23,49,52] ZnSO$_4$·7H$_2$O,[23] K$_2$Zn(CN)$_4$,[53] and ZnS),[23,52] metallic zinc,[51] Zn(CH$_3$COO)$_2$· 2H$_2$O,[19,50] and its anhydrous form.[23] In a preliminary study we demonstrated that the QCPMG experiment through its significant sensitivity enhancement relative to standard QE NMR may represent a useful tool for studies of ^{67}Zn in organometallic model compounds for metalloproteins.[11] This was demonstrated by ^{67}Zn QCPMG spectra of Zn(OOCH)$_2$·2H$_2$O and Zn-(OOCCH$_3$)$_2$(C$_3$H$_4$N$_2$)$_2$ being isotopically enriched in ^{67}Zn (90% enrichment). Obviously, the potential of studying model compounds to establish relations between anisotropic NMR param-

(48) Ng, H. N.; Calvo, C. *Can. J. Chem.* **1972**, *50*, 3619.
(49) Bastow, T. J.; Stuart, S. N. *Phys. Status Solidi B* **1988**, *145*, 719.
(50) Vosegaard, T.; Andersen, U.; Jakobsen, H. J. *J. Am. Chem. Soc.* **1999**, *121*, 1970.
(51) Bastow, T. J. *J. Phys.: Condens. Matter* **1996**, *8*, 11309.
(52) Dec, S. F.; Davis, M. F.; Maciel, G. E.; Bronnimann, C. E.; Fitzgerald, J. J.; Han, S. *Inorg. Chem.* **1993**, *32*, 955.
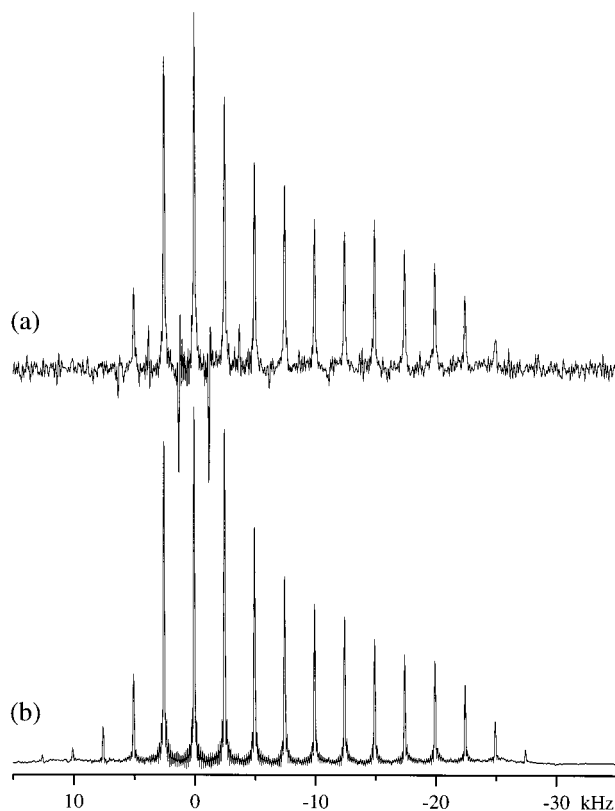(53) Wu, G.; Kroeker, S.; Wasylishen, R. E. *Inorg. Chem.* **1995**, *34*, 1595.

QCPMG NMR of Low-γ Quadrupolar Nuclei

J. Am. Chem. Soc., Vol. 122, No. 29, 2000 7085

Figure 6. Experimental (a) and simulated (b) ^{67}Zn QCPMG spectra of Zn(CH$_3$COO)$_2$·2H$_2$O. The experimental spectrum was obtained using $\tau_1 = \tau_3 = 68.0$ μs, $\tau_2 = \tau_4 = 69.4$ μs, $\tau_a = 400$ μs, $\tau_d = 122.8$ μs, $\omega_{rf}/2\pi = 58.8$ kHz, $M = 15$, a dwell time of 0.2 μs, and 72711 scans. The simulated spectrum corresponds to the parameters given in Table 2. The spectra were apodized using Lorentzian line broadenings of (a) 1 and (b) 75 Hz.

Figure 7. Experimental (a) and simulated (b−d) ^{67}Zn QCPMG spectra of Zn(Ala)$_2$·H$_2$O. The experimental spectrum was obtained using $\tau_1 = \tau_3 = 68.0$ μs, $\tau_2 = \tau_4 = 69.7$ μs, $\tau_a = 100$ μs, $\tau_d = 122$ μs, $\omega_{rf}/2\pi = 49.8$ kHz, $M = 19$, a dwell time of 0.2 μs, and 589824 scans. The simulated spectrum in part b represents the sum of the simulated spectra for sites 1 (c) and 2 (d) corresponding to the parameters in Table 2. The experimental spectrum was apodized using 150 Hz Lorentzian line broadening while 200 Hz were applied for the simulated spectra.

eters and structure would be improved considerably by the ability to investigate these compounds in natural abundance. To demonstrate that QCPMG opens up exactly this possibility, Figure 6a shows an experimental ^{67}Zn QCPMG spectrum of Zn(CH$_3$COO)$_2$·2H$_2$O with ^{67}Zn in natural abundance. Iterative fitting to the sideband intensities for this spectrum gives the C_Q, η_Q, and δ_{iso} parameters listed in Table 2 and the corresponding simulated spectrum in Figure 6b. The optimized quadrupole coupling parameters agree well with those reported earlier for Zn(CH$_3$COO)$_2$·2H$_2$O from QE NMR ($C_Q = 5.3$ MHz and $\eta_Q = 0.87$)[19] and single-crystal NMR ($C_Q = 5.34$ MHz and $\eta_Q = 0.82$).[50] We note that in the single-crystal NMR study (14.1 T), parameters for a small ^{67}Zn chemical shielding anisotropy ($|\delta_{33} - \delta_{11}| = 58$ ppm) were also obtained.[50] Although our simulation software for the QCPMG experiment allows incorporation of the CSA interaction,[26] a reliable value for the small ^{67}Zn CSA could not be extracted from the ^{67}Zn QCPMG spectrum in Figure 6a.

As a second example of natural abundance ^{67}Zn solid-state NMR, which more directly addresses bioinorganic chemistry, Figure 7 shows ^{67}Zn QCPMG spectra of Zn(Ala)$_2$·H$_2$O. Despite a relatively low signal-to-noise ratio it is immediately evident from the width of the experimental spin−echo sideband manifold in Figure 7a that the ^{67}Zn sites in this compound are characterized by very large quadrupolar couplings. Indeed, using iterative fitting the experimental spectrum can be reproduced by sideband patterns from two distinct ^{67}Zn sites characterized by δ_{iso}, C_Q, and η_Q values of 110 ppm, 11.9 MHz, 0.70 and 273 ppm, 19.0 MHz, 0.03, respectively. We note that the relatively low signal-to-noise ratio in this case prevents a precise
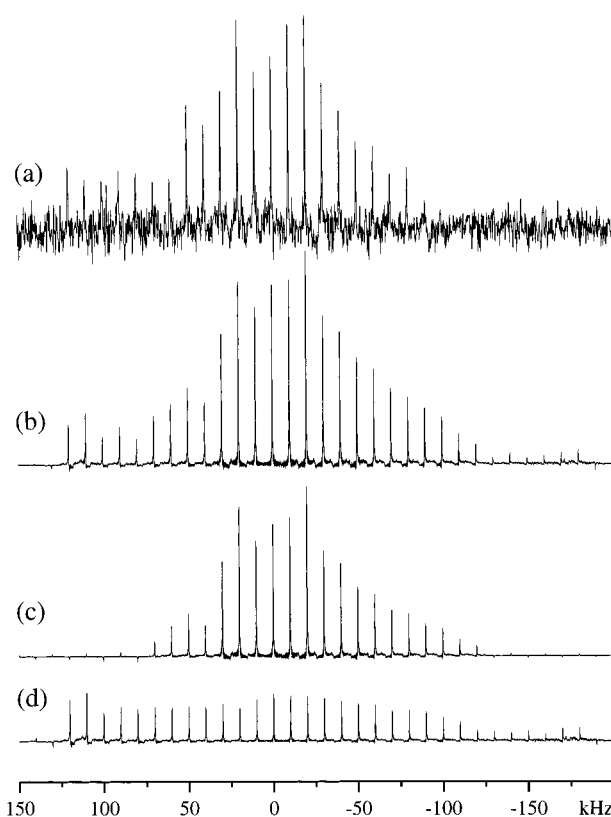
determination of these parameters. The presence of two sites agrees with a doubling of all ^{13}C resonances observed for this complex by ^{13}C MAS NMR (not shown) considering observations made for the analogous Cd-alaninate, Cd-glycinate, and Zn-glycinate complexes. For these complexes the number of distinct ^{13}C carbonyl resonances matches the number of metal sites identified by XRD.[28−31]

To the best of our knowledge ^{87}Sr solid-state NMR has so far been employed only in a single study which specifically addressed the phase transition for strontium titanate (SrTiO$_3$) around 110 K.[54] In analogy to the examples discussed above, this is most likely ascribed to experimental difficulties that may be alleviated using the QCPMG method. This is illustrated by the experimental ^{87}Sr QCPMG NMR spectra of Sr(NO$_3$)$_2$ and SrMoO$_4$ shown in Figures 8a and 9a, respectively. For Sr(NO$_3$)$_2$ the ^{87}Sr QCPMG spectrum shows a manifold of spin−echo sidebands with an envelope which over the full spectral range of about 70 kHz closely resembles the corresponding ^{87}Sr QE spectrum shown above the QCPMG spectrum in Figure 8a. Least-squares optimization of simulated to experimental QCPMG sideband intensities leads to the simulated spectrum shown in Figure 8b along with the corresponding optimized parameters in Table 2. Although the ^{87}Sr QE spectrum (experiment time 89 h) of Sr(NO$_3$)$_2$ has a considerably lower signal-to-noise ratio as compared to the QCPMG spectrum (experiment time 15.7 h), it allows for determination of the parameters $C_Q = 15.2 \pm 0.2$ MHz, $\eta_Q = 0.00 \pm 0.03$, and $\delta_{iso} = -93 \pm 4$ ppm. These

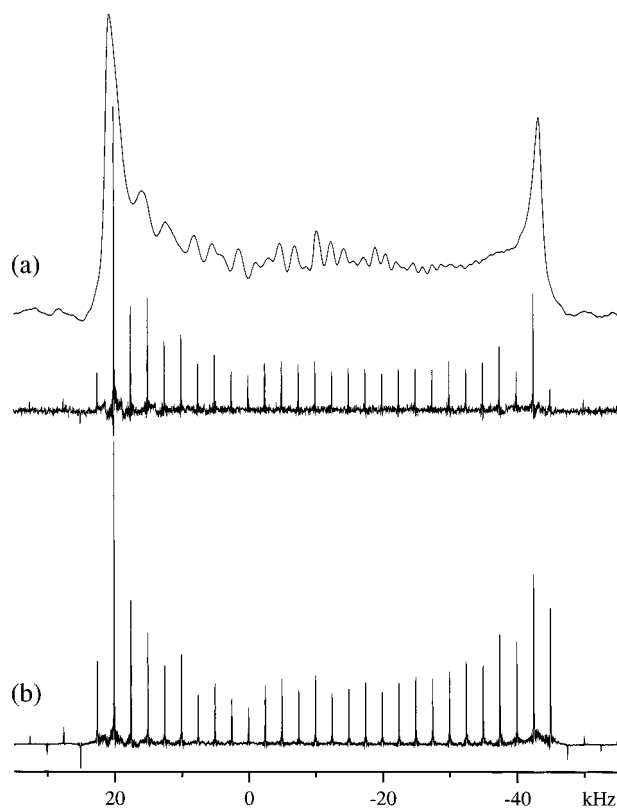(54) Weber, M. J.; Allen, R. R. *J. Chem. Phys.* **1963**, *38*, 726.

Figure 8. Experimental (a) and simulated (b) ^{87}Sr QCPMG spectra of Sr(NO$_3$)$_2$. The experimental spectrum was obtained using $\tau_1 = \tau_3 = 68.0$ μs, $\tau_2 = \tau_4 = 69.1$ μs, $\tau_a = 400$ μs, $\tau_d = 151$ μs, $\omega_{rf}/2\pi = 44.4$ kHz, $M = 30$, a dwell time of 0.5 μs, and 56576 scans. For comparison, part a includes an experimental QE spectrum recorded using $\tau_1 = \tau_2 = 100.0$ μs, and 319488 scans. The simulated spectrum corresponds to the parameters given in Table 2. The QCPMG spectra were apodized using Lorentzian line broadenings of (a) 25 and (b) 40 Hz, while a Lorentzian line broadening of 1000 Hz was used for the QE spectrum.
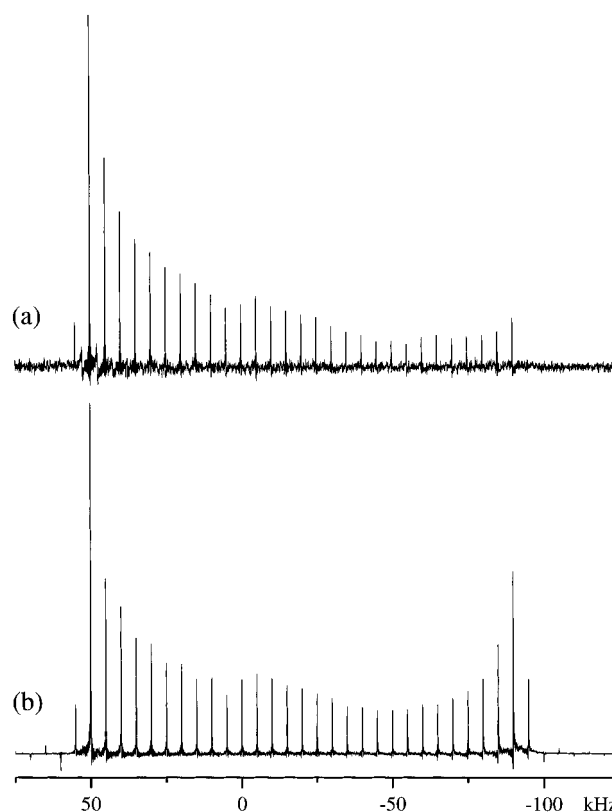

Figure 9. Experimental (a) and simulated (b) ^{87}Sr QCPMG spectra SrMoO$_4$. The experimental spectrum was obtained using $\tau_1 = \tau_3 = 140.0$ μs, $\tau_2 = \tau_4 = 141.1$ μs, $\tau_a = 200$ μs, $\tau_d = 155$ μs, $\omega_{rf}/2\pi = 46.7$ kHz, $M = 30$, a dwell time of 0.5 μs, and 70144 scans. The simulated spectrum corresponds to the parameters given in Table 2. The spectra were apodized using Lorentzian line broadenings of (a) 50 and (b) 75 Hz.

parameters are in excellent agreement with those determined from the QCPMG spectrum. We note that the utility of the standard QE spectrum in this case is highly facilitated by the axial symmetry of the electric field gradient tensor, leading to well-defined singularities for the second-order quadrupolar powder pattern which can be unambiguously determined even in case of a low signal-to-noise ratio. The observation of an axially symmetric ^{87}Sr electric field gradient tensor is in agreement with the local C_{3i} symmetry of the Sr^{2+} sites in the cubic unit cell (*Pa*3) determined for Sr(NO$_3$)$_2$ using single-crystal neutron diffraction.[55] In analogy to the observation of an anisotropic chemical shielding tensor for ^{207}Pb in Pb(NO$_3$)$_2$,[56] which is isostructural with Sr(NO$_3$)$_2$, the nonvanishing quadrupole coupling constant for ^{87}Sr in this crystal system may be explained by covalent contributions to the electric field gradient tensor at the ^{87}Sr site. Finally, the ^{87}Sr QCPMG spectrum of SrMoO$_4$ (Figure 9a) is very similar to that observed for Sr-(NO$_3$)$_2$, although a significantly larger quadrupolar coupling interaction for SrMoO$_4$ almost doubles the overall width of the spin−echo sideband envelope. An iterative fitting using the spin−echo sideband intensities from the experimental QCPMG spectrum leads to the C_Q, η_Q, and δ_{iso} parameters listed in Table 2 and the simulated spectrum shown in Figure 9b. Also in this case $\eta_Q \approx 0$, which indicates axially symmetric environments for the unique Sr^{2+} site in SrMoO$_4$. This observation is in accord with the tetragonal space group (*I*4$_1$/*a*) reported for SrMoO$_4$.[57]

Conclusions

   In conclusion, we have shown that QCPMG NMR through a very significant sensitivity enhancement relative to standard QE methods opens up the possibility for routine studies of low-γ quadrupolar nuclei in natural abundance. This has been demonstrated by ^{39}K, ^{25}Mg, ^{67}Zn, and ^{87}Sr QCPMG spectra for various solids. Obviously, the method may also be of interest for other equally demanding and exotic quadrupolar nuclei. Focusing on the biologically important ^{39}K, ^{25}Mg, and ^{67}Zn cations, it is anticipated that the QCMPG method, through accessibility of these nuclei in natural abundance, will find widespread application as a tool to establish relations between anisotropic nuclear spin interactions and structural parameters in model complexes for metalloproteins. This is of fundamental importance for solid-state NMR to become a more general tool for studying metal binding in biological macromolecules.

   (55) Nowotny, H.; Heger, G. *Acta Crystallogr.* **1983**, *C39*, 952.
   (56) Lutz, O.; Nolle, A. *Physik* **1980**, *B36*, 323.

   (57) Egorov-Tismenko, Y. K.; Simonov, M. A.; Belov, N. V. *Kristallografiya* **1967**, *12*, 511.